Article

Not peer-reviewed version

Unexpected Hepatoprotective Effects of the Neuroprotector Lithium Ascorbate in a Model of a "Western" Diet with Iron Overload and Multiple Organ Pathology

Ivan Torshin , Olga Gromova * , Tatiana Bogacheva , Vadim Demidov , Vyacheslav Rastashansky

Posted Date: 20 September 2024

doi: 10.20944/preprints202409.1645.v1

Keywords: neuroprotectors; lithium therapy; fatty liver disease; animal models; hepatoprtection; iron overload; hemosiderosis; chemoinformatics; intelligent data analysis (data mining); lithium ascorbate

Article

Unexpected Hepatoprotective Effects of the Neuroprotector Lithium Ascorbate in a Model of a "Western" Diet with Iron Overload and Multiple Organ Pathology

Ivan Yu. Torshin [1], Olga A. Gromova [1,*], Tatiana E. Bogacheva [2], Vadim I. Demidov [2,*] and Vyacheslav V. Rastashansky [3,*]

[1] Federal Research Center "Computer Science and Control" of Russian Academy of Sciences, Moscow, Russia
[2] Ivanovo State Medical University, Ivanovo, Russia
[3] LLC Normotim, Moscow, Russia
* Correspondence: unesco.gromova@gmail.com (O.A.G.); 13vid@mail.ru (V.I.D.); vvrast@mail.ru (V.V.R.)

Abstract: Lithium ascorbate (LiAsc) is a non-toxic lithium salt (LD50>5000 mg/kg) with normothymic and neuroprotective properties. Chemoreactomic modeling of LiAsc predicted possible hepatoprotective effects which were tested here on a rat model of a non-alcoholic fatty liver disease (NAFLD) with multiorgan pathology caused by combined intake of excess saturated fats (palm oil), carbohydrates (fructose) and inorganic iron salt (ferrous sulfate). Dynamics of biochemical parameters (biomarkers of liver function, kidneys, hematopoiesis, inflammation, thrombus formation, etc.) and histological evidence of hemosiderosis in the model upon reproduction of the model are described. Experimental confirmations of the hepatoprotective effects of LiAsc were obtained. Comparison of the effects of LiAsc with the effects of myoinositol (a substance with known hepatoprotective properties) shown a number of differences in pharmacological action. Both LiAsc and MI lowered ferritin, transferrin saturation, serum iron, AST, ALT, serum creatinine, leukocytes (LiAsc to a greater extent) and normalized lowered serum protein and glomerular filtration rate. However, only LiAsc lowered heightened reticulocytes (absolute and fraction) and platelets towards the corresponding reference intervals, normalized levels of vitamin B12 in blood and lowered the number of Kupffer cells in liver that were overloaded with iron (contained Prussian blue in morphometric studies). In a clinical perspective, hepatoprotective properties of a neuroprotector and it's potential to reduce hemosiderosis might be useful for treating patients with hepatic encephalopathy.

Keywords: neuroprotectors; lithium therapy; fatty liver disease; animal models; hepatoprtection; iron overload; hemosiderosis; chemoinformatics; intelligent data analysis (data mining); lithium ascorbate

1. Introduction

Lithium ions inhibit glycogen synthetase kinase-3β (GSK3β) and other target proteins thus simulating a rise in the levels of endogenous neurotrophic factors and neuroprotective effects of lithium salts. A complex experimental approbation of pharmacological properties of a lithium salt with an organic anion, lithium ascorbate (LiAsc), was previously reported on the pages of this journal [1]. The neurocytological study indicated direct neuroprotective effects of LiAsc on cultured neurons under glutamate stress. The biodistribution studies in rats indicated accumulation of lithium ions in a sort of "depot" consisting of brain, aorta and femur. Studies of LiAsc (5, 10, 30 mg/kg) performed on a model of alcohol intoxication in rats shown the reduction of ischemical brain damage and the increase in preservation of the myelin sheaths of the neurons. Extremely low acute toxicity

 doi:10.20944/preprints202409.1645.v

(LD50>5000 mg/kg) and even a moderate antitumor effect contribute favorably to the safety profile of LiAsc [1].

The pharmacological action of the LiAsc is not likely to be restricted only to the above-mentioned effects. For example, chemoreactomic modeling of LiAsc, conducted using modern data mining technologies, allowed us to obtain estimates of the hemodynamic and anti-inflammatory properties of the substance. In particular, LiAsc might be characterized by anti-inflammatory action (modulation of prostaglandin metabolism, lipopolysaccharide-induced TNF-alpha production), demonstrate anticoagulant, antihyperlipidemic and antihyperglycemic effects whereas lithium carbonate (Li_2CO_3) was not predicted to exhibit any of the above. Chemoreactomic analysis indicated that ascorbate-anion in the LiAsc may be much more effective than nicotinate and oxybutyrate anions in the corresponding lithium salts for reducing glucose tolerance (activating the PPAR receptor, a known target protein for antidiabetic drugs) [2]. The latter effect was, in fact, confirmed in a comparative study of the effects of LiAsc and Li_2CO_3 in the alloxan diabetes model: the use of LiAsc was statistically significantly associated with an increased animal survival and decreased hyperglycemia [3].

Another study dealing with chemoreactomic modeling indicated possible benign influence of LiAsc on 38 commensal bacteria of human microbiota (including various types of bifido- and lactobacilli) and on the values of minimum inhibitory concentrations (MIC) for 120 pathogenic bacteria. On average over 38 representative of commensals LiAsc slightly more significantly supported the growth of all commensal bacteria (AUC=0.57±0.15) than lithium comenate (AUC=0.47±0.17), lithium nicotinate (AUC=0.45±0.22), lithium oxybutyrate (AUC=0.22±0.17), lithium aspartate (AUC=0.31± 0.14) and lithium orotate (AUC=0.50±0.21). In the case of pathogenic microorganisms, MIC values were significantly lower for LiAsc (4.50±3.69 μg/ml) than for comenate (6.31±5.58 μg/ml), nicotinate (10.98±9.37 μg/ml), oxybutyrate (7.45±4.73 μg/ ml) and aspartate (6.37±4.71 mcg/ml) anions of the lithium salts. The Li_2CO_3, again, did not show any useful properties in this *in silico* study [4].

Thus, the results of mathematical modeling and of a few of experimental studies indicate a wider range of pharmacological properties of LiAsc than just neuroprotection. In this work we describe the hepatoprotective effects of LiAsc which we tested on a rat model of non-alcoholic fatty liver disease (NAFLD) with multiorgan pathology caused by combined intake of excess saturated fats, carbohydrates and inorganic iron salt.

NAFLD is a widespread disease that occurs as a result of dietary disorders (excess fats and simple carbohydrates, micronutrient deficiencies), toxic load on the liver, etc. A diet with excessive palm oil consumption contributed to the development of histologically confirmed steatohepatosis, characterized by fatty degeneration of hepatocytes localized predominantly in the periportal zone of the liver lobule [5]. Combined with other factors (for instance, with iron overload due to iatrogenic or genetic causes), NAFLD develops faster and progresses to multiorgan pathology associated with damage to the liver, kidneys, heart, brain and other organs. Iron overload is one of the complications of NAFLD most difficult to treat: tissue iron overload initiates the formation of reactive oxygen species (ROS) and oxidative stress, insulin resistance, and proinflammatory reactions [6,7].

It is well known that NAFLD and liver iron overload are aggravated by high fructose consumption [8]. Excess dietary fructose stimulates rapid accumulation of intrahepatic fat, oxidative stress, mitochondrial dysfunction of hepatocytes [9] and development of insulin resistance [10]. It is known that patients with NAFLD and/or obesity consume almost 2 times more soft drinks compared to healthy controls [11–15]. Therefore, the use of a fructose-overloaded diet is also an important direction for the development of NAFLD models.

To our knowledge, a NAFLD model in rats with iron overload, induced by a diet rich in palm oil and fructose, was not earlier described. The first objective of this work was to develop a biochemically and histologically confirmed model of NAFLD with iron overload against the background of excessive consumption of palm oil and fructose.

The second objective of the study - to compare the effectiveness of the hepatoprotective properties of LiAsc in comparison with a substance with known hepatoprotective properties -

 doi:10.20944/preprints202409.1645.v

myoinositol (MI). Inositol-dependent proteins are involved in supporting the activity of the cardiovascular system, kidneys, liver, nervous tissue, immunity and sugar metabolism (primarily, the insulin signaling cascade) and pharmacological properties of MI include hepato- and nephroprotection [16,17].

2. Results

Chemoreactomic modeling in silico indicated the possibility of lithium ascorbate having hepatoprotective effects. As a result of conducting a set of experimental studies in vivo it was established that both the reproduction of the NAFLD model with iron overload and the therapeutic approaches used (LiAsc, MI) resulted in a complex interrelated changes in many biochemical blood indicators (parameters). Therefore, for a more complete description of the results of the animal studies, a special form of data presentation was used: profile diagrams of the normalized values of all the studied indicators.

2.1. Results of chemoreactomic modeling of hepatoprotective properties of several lithium salts

As an input to the algorithms were used chemical structures of the lithium ascorbate, myoinositol and lithium carbonate. Chemoreactomic screening of the lithium salts included calculation of the 486 hepatoprotective activities the training/validation data for which were extracted from PubChem (see Methods). After calculations only those activities were left that shown statistically different values for at least one of the substances (44 activites). A selection of the most prominent differences in hepatoprotective activities is presented in the Table 1. Apparently, LiAsc might show hepatoprotective properties comparable to those of MI.

Table 1. Results of chemoreactomic analysis of the lithium salts and myoinositol in rats. "Const.", The common name for the type of investigational pharmacological constant ("IC50"); "Error" - the error of the estimated biological constant; "Unit", units of measurement.

Activity	Const	Unit	Error	LiAsc	MI	Li_2CO_3
Hepatoprotective activity against D-GalN-induced cytotoxicity in primary cultured rat hepatocytes at 30 uM dose	-	%	8.2	20.8	25.5	0
Hepatoprotective activity assessed as inhibition of D-galactosamine-induced cytotoxicity (100 uM of substance, MTT assay, % relative to untreated control)	-	%	5.3	17.2	28.2	0
In vitro inhibition of Acyl coenzyme A:cholesterol acyltransferase in rat hepatic microsomes (AIV assay)	IC50	nM	50.7	225.4	41.8	>10000
In vitro inhibition of rat liver HMG-CoA reductase	IC50	nM	19.4	122.0	97.0	>10000
In vivo lowering of blood glucose levels in Zucker diabetic rats (postprandial glucose, day 3, after 300 uM/kg *per os*)	-	%	7.2	46.2	46.0	0

 doi:10.20944/preprints202409.1645.v

2.2. Preliminary studies, general observations of the model and of the effects of the substances

Prior to conducting the main series of experiments as described in methods we attempted a few preliminary experiments for an expert approbation of the putative hepatoprotective properties of LiAsc (30 mg/kg/day of elemental lithium), Li_2CO_3 (30 mg/kg/day of lithium) and of sodium ascorbate (30 mg/kg/day of elemental sodium). These studies were conducted during development of the proposed NAFLD model and allowed us to conclude that any further study of Li_2CO_3as a hepatoprotector would be a waste of resources. In fact, lithium carbonate did not apparently affect the state of the liver tissue and aggravated the condition of kidneys. Sodium ascorbate did not show any toxic influences but it's hepatoprotective effects were apparently weaker than those of LiAsc and MI with the doses used. Hence, the further studies (that included a detailed biochemical characterization of the groups and the histological data) were performed only for LiAsc (30 mg/kg/day) and MI (400 mg/kg/day).

Preliminary studies and the main sequence of experiments included qualitative observation of the general state of the animals. Animals of the first group (intact control) had clean, white, smooth fur. The animals were active, non-aggressive, and their food and water consumption was not below the established feeding standards. Normal muscle tone was observed and no signs of aggression were noted.

When reproducing the model (first two days) in the second, third, fourth groups the animals shown clean shiny fur and skin without external signs of disease. Rats were active, food consumption was not below the feeding standards. From the 3rd day after the model was reproduced, the animals began to consume less food, drink more fructose solution, shown signs of polyuria (wet, “ruffled” fur, necessity of frequent change of sawdust filler), dehydration (dry and dull skin and mucous membranes of the eyes) and of decreased motor activity. At the same time the rats became more aggressive: for example, on the 10th day of the study, a number of rats in the three groups had a torn out tuft of fur on their sides, it was harder for researchers to handle the rats etc.

In the third (LiAsc) and fourth (MI) groups animals from the 15th day forth shown an increase in motor activity and normalization of the muscle tone. In the fourth week of the study, signs of polyuria and dehydration were not were detected in these two groups; the rats' fur was clean and dry. The rats became calmer, less aggressive and made good contact with the researcher. The consumption of food and water was not lower than the established feeding norms. Such vivid dynamics was not observed in the control group and in the animals that received lithium carbonate or sodium ascorbate during the preliminary studies.

2.3. Analysis of profile diagrams of normalized values of the studied indicators

Profile diagrams of normalized values of all studied parameters allowed us to describe the dynamics and differences between groups in somewhat holistic a manner. As is known, the values of various biomedical parameters can lie in different ranges (0-1 mmol, 50-500 ng/ml, etc), therefore they cannot always be presented on one diagram. Analysis of the normalized profile diagrams of biochemical parameter values during model reproduction (Figure 1) indicates a sharp increase in ferritin (indicator 1), a sharp drop in indicators 8-11 (erythrocytes, hemoglobin, hematocrit, mean corpuscular volume), an increase in indicators 12-17 (mean corpuscular hemoglobin content, mean corpuscular hemoglobin concentration, platelets, folates), a drop in serum protein, etc.

 doi:10.20944/preprints202409.1645.v

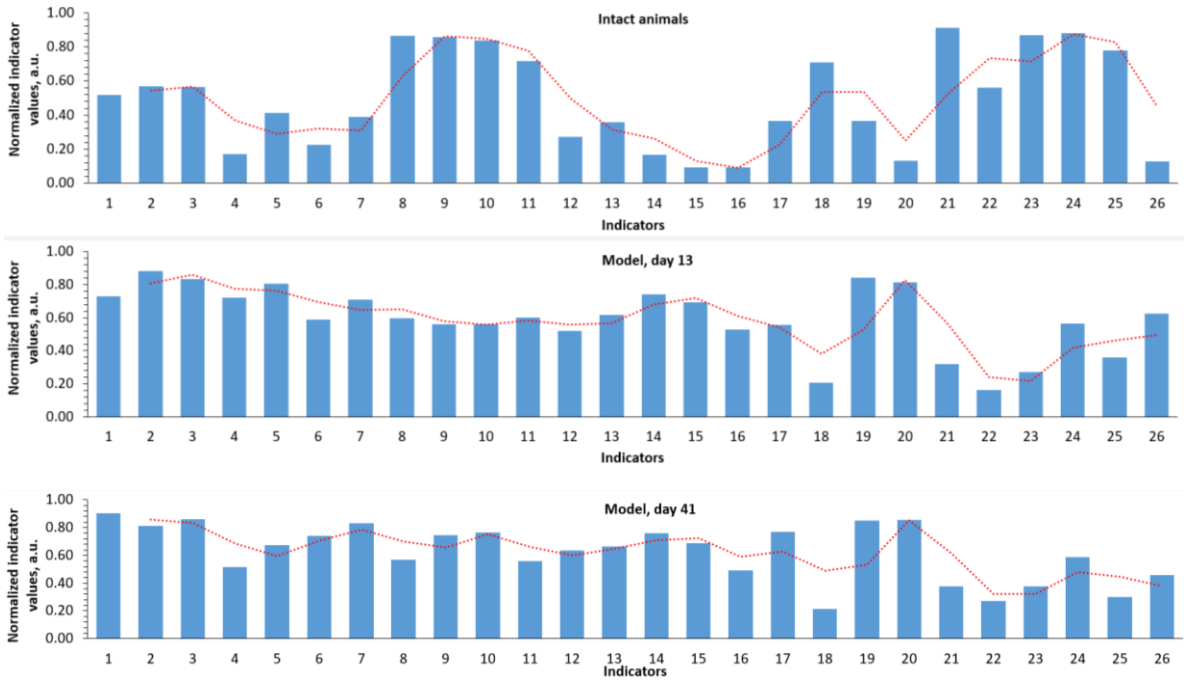

Figure 1. Normalized profiles of biochemical indicator values during reproduction of the developed NAFLD model. The red dashed-dotted line describes the profile of changes in all indicators/parameters as a whole. 1 - Ferritin, μg/L; 2 - Transferrin saturation coefficient with iron, %; 3 - Serum iron, μmol/L; 4 - Reticulocytes, %; 5 - Reticulocytes, bln/L; 6 - Reticulocyte fraction, %; 7 - Leukocytes, bln/L; 8 - Erythrocytes, trln/L; 9 - Hemoglobin, g/L; 10 - Hematocrit, %; 11 - Mean corpuscular volume, fL; 12 - Mean hemoglobin content in erythrocytes, pg; 13 - Mean hemoglobin concentration in erythrocytes, g/L; 14 - Platelets, bln/l; 15 - Mentzer index; 16 - Sirdah index; 17 - folates, nmol/l; 18 - Total serum protein, g/l; 19 - AST, U/l; 20 - ALT, U/l; 21 - Serum creatinine, μmol/l; 22 – Glomerular filtration rate; 23 - Total bilirubin, μmol/l; 24 - Direct bilirubin, μmol/l; 25 - Vitamin B12, pg/ml; 26 - Kupffer cells, whose cytoplasm contains Prussian blue.

The normalized profiles of biochemical parameter values clearly characterize the differences when using MI and LiAsc on day 41 (Figure 2). MI action was characterized by a decrease in iron metabolism parameters (indicators 1-3), an increase in parameters 4-6 (reticulocytes, %; reticulocytes, reticulocyte fraction), a sharp drop in AST, ALT (indicators 19, 20). The profile of the effect of LiAsc combined a decrease in iron metabolism parameters with a decrease in the average corpuscular volume, hemoglobin content in the erythrocyte, platelets (parameters 11-14) against the background of a marked increase in the glomerular filtration rate (GFR).

Analysis of the normalized profiles of biochemical parameters (Figure 2) allowed us to obtain a more comprehensive picture of the differences in the effects of the studied approaches to iron overload therapy than using any individual parameters (AST/ALT, blood iron levels, etc.). We divided components of these profiles into three segments: iron metabolism parameters, general blood test parameters, and biochemical parameters of multiple organ dysfunction.

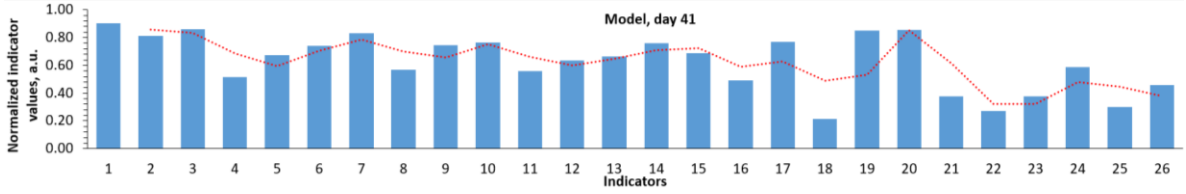

 doi:10.20944/preprints202409.1645.v

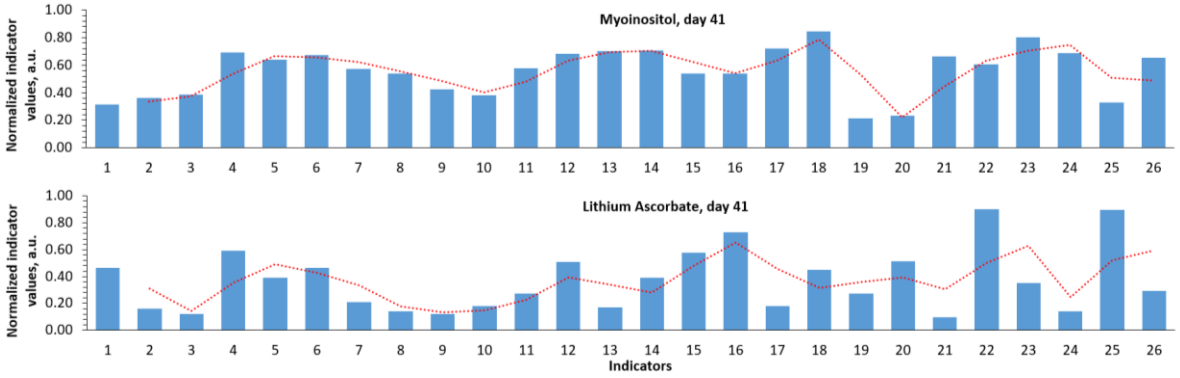

Figure 2. Normalized profiles of biochemical parameter values using different approaches to therapy. Parameter designations are as in Figure 1; the slide for day 41 of the model was repeated from Figure1 for the sake of convenience of visual comparisons.

2.3.1. Iron metabolism indicators

Analysis of iron metabolism indicators (Figure 3A) shown the development of iron overload during the reproduction with subsequent normalization of blood iron levels. It is evident from the profiles that the values of the three "fast" iron metabolism parameters (ferritin, transferrin saturation coefficient, serum iron) increased sharply in the model compared to intact controls: ferritin from 201±45 μg/L to 229±13 μg/L (day 13, P<0.0001) and further to 254±12 μg/L (model, day 41, P<0.0001). Transferrin saturation coefficient values increased from 57±8% (intact) to 88±15% (day 13, P<0.0001) and slightly decreased at day 41 81±27% (P<0.0001). Serum iron levels increased from 28±5 μmol/L (intact) to 50±10 μmol/L on days 13 and 41 (P<0.0001).

Treatment with LiAsc and MI resulted in a significant decrease in ferritin on day 41 (MI: 173±52 μg/L, LiAsc: 203±4 μg/L, both P<0.0001) so MI contributed to a greater decrease in ferritin. In case of transferrin saturation coefficient LiAsc had the greatest effect on day 41 (MI: 36±9%, LiAsc: 16±8%, all P<0.00005) and on serum iron (MI: 23±5 μmol/L, LiAsc: 13±4 μmol/L, both P<0.0001).

At the same time, the nature of changes in the levels of the "slower" hemoglobin indicator in the blood differed significantly from changes in the "fast" indicators: when reproducing the model, hemoglobin levels significantly decreased (intact 148.8±4.5 g/l, model day 13: 130.2±17.5 g/l, P=0.02), recovering by day 41 (143.2±5.7 g/l). MI and LiAsc did not contribute to the recovery of hemoglobin levels (P>0.1).

Histomorphometry data (number/percentage of Kupffer cells, in the cytoplasm of which staining for iron was identified) represent another independent indicator of the efficiency of iron excess removal by LiAsc and MI. Compared with intact group (16.7±1.4) the number of cells stained with Prussian blue after reproducing the model increased significantly already by day 13 (24.2±3.1, P=0.00048), decreasing insignificantly by day 41 (21.7±3.9). MI did not significantly influence the number of such cells (25.2±3.5) while LiAsc, on the contrary, contributed to the decrease of the Prussian-blue-stained Kupffer cells (18.8±2.5, P=0.1 when compared with intact group).

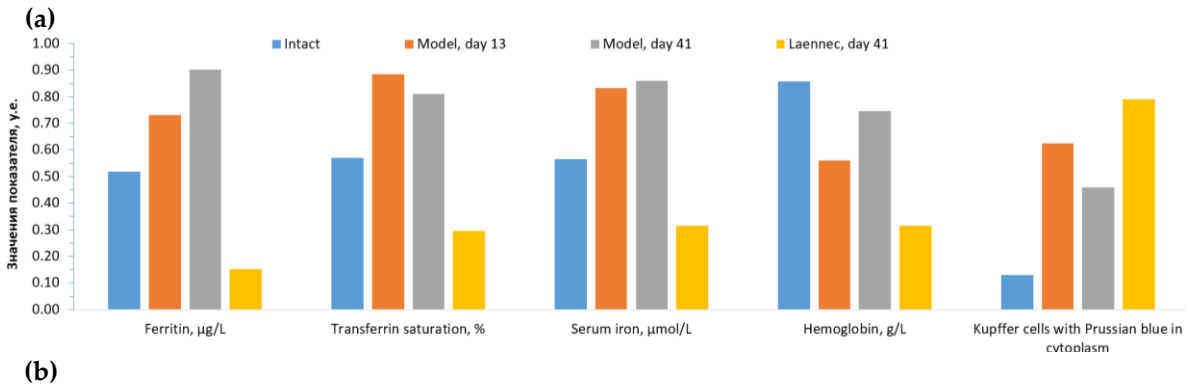

 doi:10.20944/preprints202409.1645.v

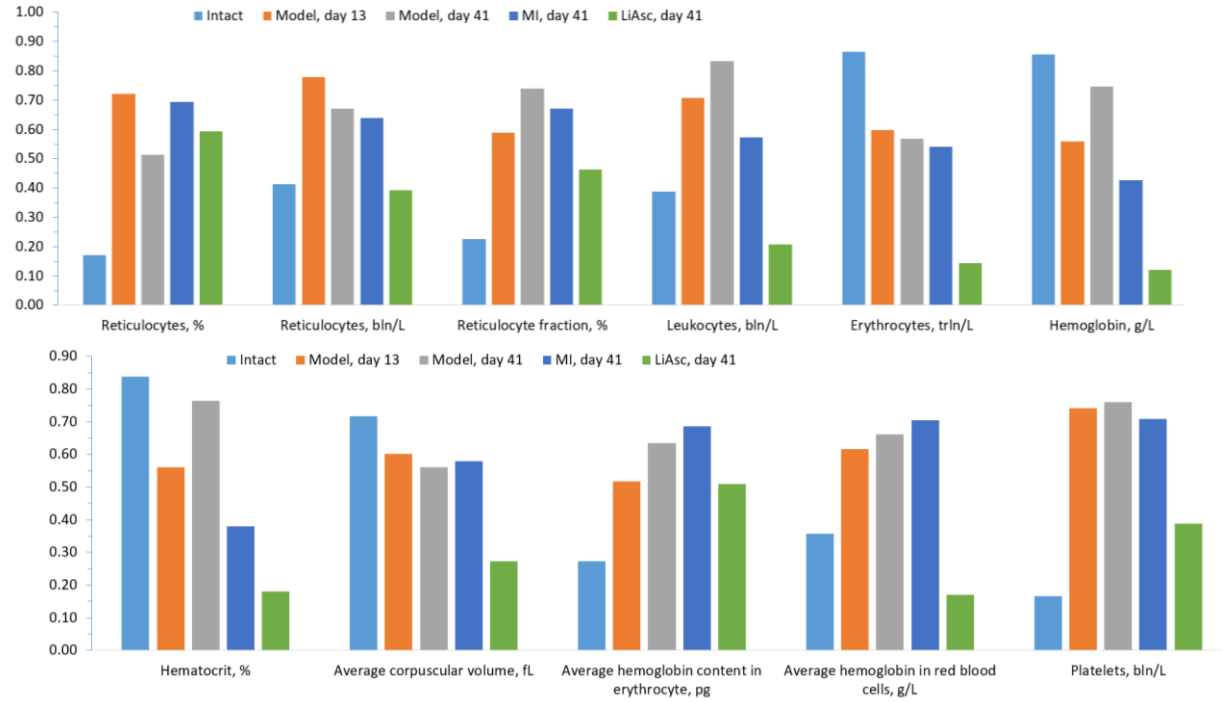

(c)

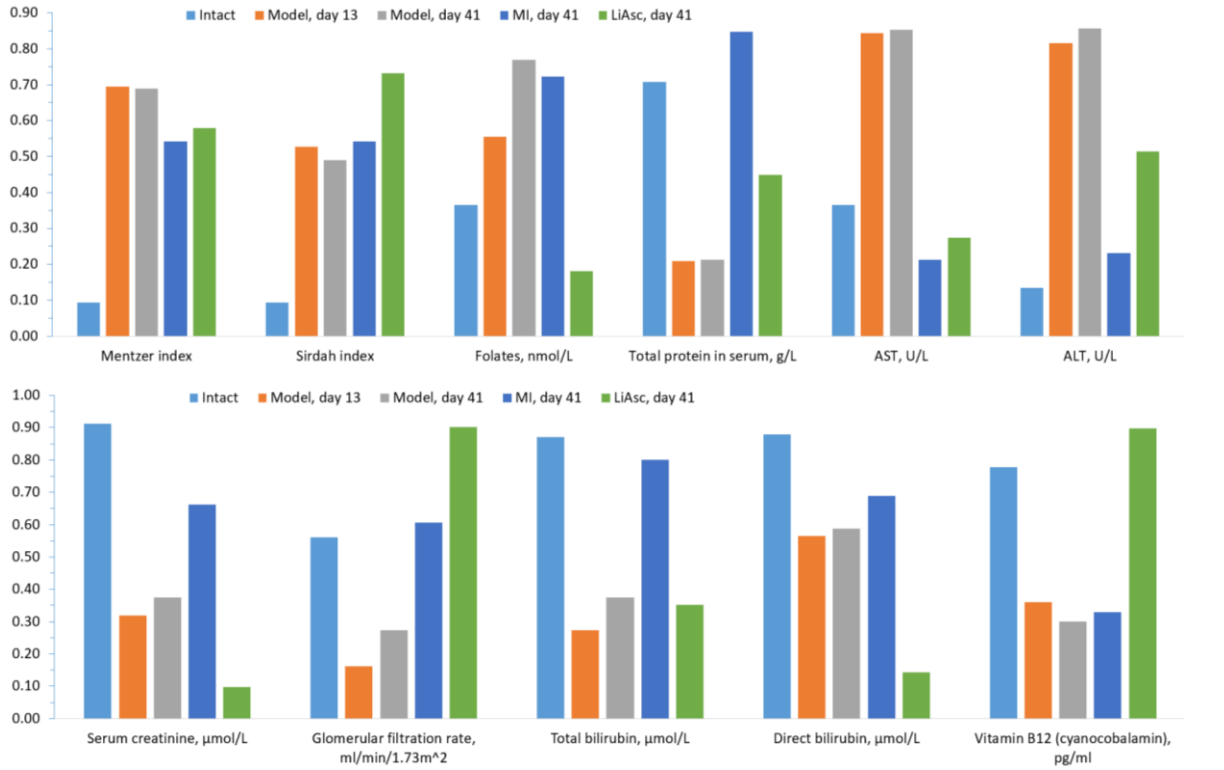

Figure 3. Profiles of biochemical parameters of the studied groups. (a) Iron metabolism parameters, (b) general blood test parameters, (c) multiple organ dysfunction parameters.

2.3.2. Indicators of the general blood test

When reproducing the model, an observable decrease in the total number of red blood cells was noted (intact 8.7±0.8 trln cells/l, model day 13 7.4±1.2 trln/l, P=0.022, day 41: 7.1±1.4 trln/l). At the same time, the mean corpuscular volume did not change (intact 52.6±1.4 fl, model, days 13/41 - 50±5 fl); a significant increase in the average amount of hemoglobin in the erythrocyte was noted (intact 15.8±0.3 pg, model, day 13/41 16.2±0.1 pg, P=0.013) and a trend towards an increase in the average

 doi:10.20944/preprints202409.1645.v

concentration of hemoglobin in the erythrocyte (intact 286±31 g/l, model, days 13/41 - 308±6 g/l, P=0.06).

The studied substances differed significantly in their effects on the erythrocyte parameters. While MI had no significant effects even on day 41, the use of LiAsc resulted in a significant decrease in the mean red blood cell volume (39.3±16 fL, P=0.05) against the background of a decrease in the mean amount of hemoglobin in the red blood cell towards the normal range (273±17 g/L, P=0.001). MI did not have a significant effect on the total number of red blood cells (P>0.07).

All three indicators characterizing various aspects of the reticulocyte content in the blood (% of reticulocytes, reticulocyte content, reticulocyte fraction) increased significantly after reproducing the model (Figure 1): increased were percentage of reticulocytes (intact 3.1±0.7%, model, d.13 5.2±1.0%, P=0.00115), total reticulocyte count (intact 288±61 bln/l, model, d.13 433±116 bln/l, P=0.014), reticulocyte fraction (intact 43.3±6.1%, model, d.13 54.5±7.0%, P=0.007) with a small and statistically insignificant decrease in all three parameters by day 41 (P>0.08). On day 41 MI did not have any effect on all the three parameters of reticulocytes (P>0.1) whereas LiAsc stimulated a decrease in total reticulocyte count and reticulocyte fraction towards the normal range (reticulocyte count 291±45 bln/L, P=0.0052; reticulocyte fraction 51±6%, P=0.0275).

2.3.3. Biochemical indicators of multiple organ dysfunction

Analysis of the other biochemical parameters (Figure 3B) associated with the characterization of multiple organ dysfunction (inflammation and thrombus formation, renal functon, liver function) indicated positive effects of both LiAsc and MI.

Inflammation and thrombus formation. Levels of leukocyte (white blood cells, WBC) in intact animals were 4.6±1.3 bln cells/L, and in the model they increased by an average of +1.6 bln/L by day 13 (6.2±1.0 bln/L, P=0.022) with an upward trend by day 41 (6.9±0.8 bln/L, P=0.067). Both treatment approaches resulted in a decrease in WBC levels toward the normal range observed in intact animals. MI normalized abnormally elevated WBC levels (5.4±0.6 bln/L, P=0.0018). LiAsc resulted in a more pronounced decrease in leukocytes on day 41 (3.7±0.6 bln/l, P<0.0001), with a trend towards a significant difference from the values for intact animals (P=0.068).

Platelet levels were 509.7±121.6 bln/L in the intact group and increased to 860.8±156.2 bln/L (P=0.00083) on day 13 after model reproduction, with a non-significant decrease by day 41 (820.2±50.5 bln/L, P>0.1). LiAsc contributed to the normalization of platelet levels (681±23 bln/L, P=0.00024), and MI showed a decrease, but not significant (813±78 bln/L, P>0.1).

Renal function. Serum creatinine and glomerular filtration rate (GFR) are indicators of the renal function. Upon the model reproduction creatinine and GFR levels decreased significantly by day 13 without significant changes by day 41, indicating the development of renal damage due to iron overload against the background of lipid and carbohydrate metabolism overload. Serum creatinine fell from 35.7±1.2 μmol/L in intact animals to 22.5±2.4 μmol/L in the model on day 13 (P<0.00001), with no change by day 41 (23.3±1.4 μmol/L).

Both LiAsc and MI contributed to the restoration of renal function. The effect of MI was quite noticeable, with creatinine levels returning to near baseline (30.3±5.1 μmol/L, P=0.0093), with no significant differences from intact animals. The effect of LiAsc on day 41 was even more pronounced (19.2±1.2 μmol/L, P=0.00011).

In intact animals, the GFR was 169±5 ml/min/1.73 m^2, and when reproducing the model, it dropped to 142.4±12.3 ml/min/1.73 m^2 on day 13 (P=0.0011), with a partial improvement on day 41 (154.1±7.1 ml/min/1.73 m^2, P=0.04). MI and LiAsc contributed to a significant restoration of GFR. Thus, MI led to an increase in GFR up to 176.7±24.8 ml/min/1.73 m^2 (P=0.038), and LiAsc – up to 198.1±8.5 ml/min/1.73 m^2 (P<0.00001), which was even higher than in intact animals (P=0.00005).

Liver function. AST levels were 114.9±27.3 U/L in intact animals. When reproducing the model in groups 2-4, a more than twofold increase in AST was noted to 299.9±27.9 U/L (P<0.000001) on day 13, with no changes by day 41 (301.3±30.3 U/L). MI and LiAsc contributed to achieving AST levels similar to those in intact animals on day 41 (MI 94±35 U/L, P<0.000001; LiAsc 121.9±2.0 U/L, P=0.000013).

 doi:10.20944/preprints202409.1645.v

ALT levels changed similarly: compared with intact (22.8±3.2 U/L), model reproduction resulted in a significant increase in ALT on day 13 (54.1±9.8 U/L, P=0.00014), with no change by day 41 (58.7±5.5 U/L). LiAsc (34.8±1.7 U/L, P=0.000027) contributed to ALT normalization. MI, reducing ALT to 25.8±3.8 U/L (P<0.000001), stimulated ALT restoration to levels characteristic of intact animals (P>0.1 when compared with intact, 22.8±3.2 U/L).

Model reproduction resulted in a decrease in total protein levels at day 13 (intact 57.0±4.7 g/L, model 45.5±5.8 g/L, P=0.002), with no change at day 41 (46.2±4.6 g/L). Both agents had a positive effect on liver biosynthetic function, promoting recovery of total protein levels by day 41 (MI 60.7±3.7 g/L, P=0.0001; LiAsc 52.5±1.0 g/L, P=0.01).

When reproducing the model, blood folate levels showed an upward trend by day 13 (62.4±5.6 nmol/L, intact 52.5±15.0 nmol/L, P=0.078). The dynamics of the increase in folate levels reached statistical significance by day 41 (67.6±3.1 nmol/L, P=0.043). By day 41, MI had no significant effect (67.4±7.8 nmol/L), and LiAsc contributed to a decrease to the normal range (49.6±2.9 nmol/L, P<0.000005 when compared with model at day 41, P>0.1 when compared with intact).

When reproducing the present model, the previously described increase in folate levels was combined with a decrease in blood vitamin B12 levels (intact 264.5±58.1 pg/mL, model, day 13 190.5±7.1 pg/mL, P=0.013, no dynamics by day 41 - 189.7±4.8 pg/mL). MI did not significantly affect B12 levels (165.0±40.1 pg/mL, P=0.096). LiAsc promoted normalization of vitamin B12 levels, to levels significantly higher than in intact animals (325.3±23.1 pg/mL, P<0.00001 when compared with model on day 41, P<0.001 when compared with intact).

2.4. Histological confirmation of the model and of the effects of the substances

The histological studies conducted included analysis of the intact control group, effects of model reproduction on liver, kidneys, brain and heart, the description of the effects of the myoinositol treatment and of the lithium ascorbate treatment of the NAFLD model with iron overload.

2.4.1. Histological study of the intact control group

In all observations of the intact control group, the microscopic structure of the liver tissue corresponded to the normal state. Within a single liver lobules, with the preservation of histoarchitecture, hepatocytes had the usual configuration and uniform coloring with a uniform distribution of ultrastructures in the cytoplasm without the formation of Prussian blue (Figure 4A), uniform perfusion of sinusoids was observed both in the central and periportal zones, and single lymphocytes were present in the stroma of the portal tracts (Figure 4B).

The renal cortex showed the usual structure of the glomeruli with a normal level of blood perfusion and free mesangial space. Nephrocytes within the convoluted proximal and distal tubules were not damaged (Figure 4C).

The brain of the control group rats had a normal perfusion level without signs of erythrocyte aggregation in the capillaries and edema of the nervous tissue. The neurons had the usual shape and size with clear contours of the nuclei. In the cytoplasm of the pyramidal neurons of the cortex of the forebrain hemispheres, the Nissl lumps were uniformly distributed (Figure 4D). In the myocardium of the left ventricle, oriented contractile fibers with preserved transverse striation were observed (Figure 4E).

 doi:10.20944/preprints202409.1645.v

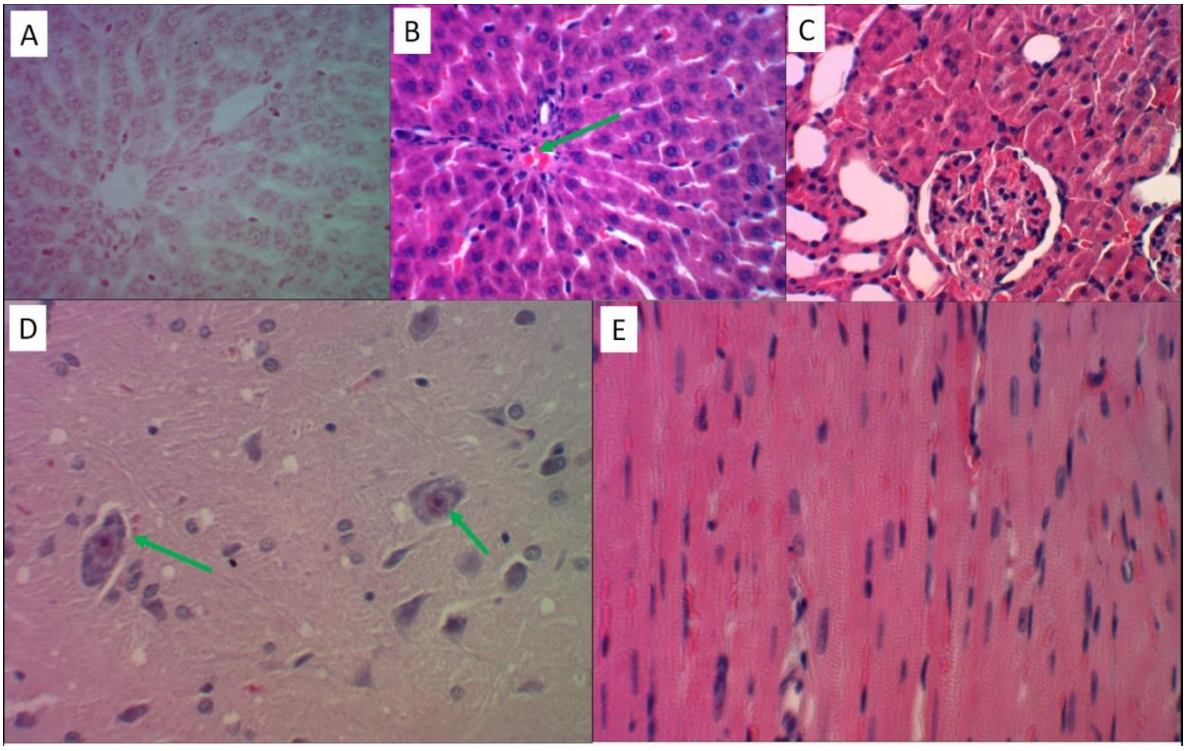

Figure 4. Histological analysis of various organs of intact animals. All slides magnified x480. Stained with Perls reaction (A), hematoxylin and eosin (B-E). A) Structure of an unchanged liver lobule with trabecular arrangement of hepatocytes. B) Single lymphocytes in the stroma of the portal tract against the background of uniform perfusion of all parts of the liver lobule. C) The renal glomerulus has a lumen of the capsule and free mesangium, epithelial cells of the proximal and distal convoluted tubules with homogeneous staining of the cytoplasm. D) Pyramidal neurons of the usual configuration with uniform distribution of Nissl lumps in the cytoplasm. E) Contractile fibers of uniform staining and thickness, anisotropic disks are visible.

2.4.2. Model reproduction, the effects on liver

After 12 days of administration of ferrous sulfate, palm oil, and fructose solution, accumulation of iron-containing compounds in the Disse space, cytoplasm of hepatocytes, and Kupffer cells of the periportal zone of liver lobules was observed in the liver (Figure 5A). In the central sections of the liver lobule, hepatocytes contained small lipid droplets (Figure 5B). After 41 days from the beginning of the experiment, the iron-containing substrate in the liver was redistributed and actively accumulated in the cytoplasm of Kupffer cells (Figure 5C) and between the connective tissue fibers of the liver capsule (Figure 5D), with most hepatocytes being free of Prussian blue. Progression of fatty degeneration of hepatocytes with the formation of large vacuoles with lipids in their cytoplasm was observed (Figure 5E). In most observations, the stroma of the portal tracts had an inflammatory cell infiltrate consisting mainly of T-lymphocytes and eosinophils (Figure 5F, G). The histological picture corresponded to a moderate expression of the inflammatory reaction both by day 13 and by day 41 after reproducing the model.

 doi:10.20944/preprints202409.1645.v

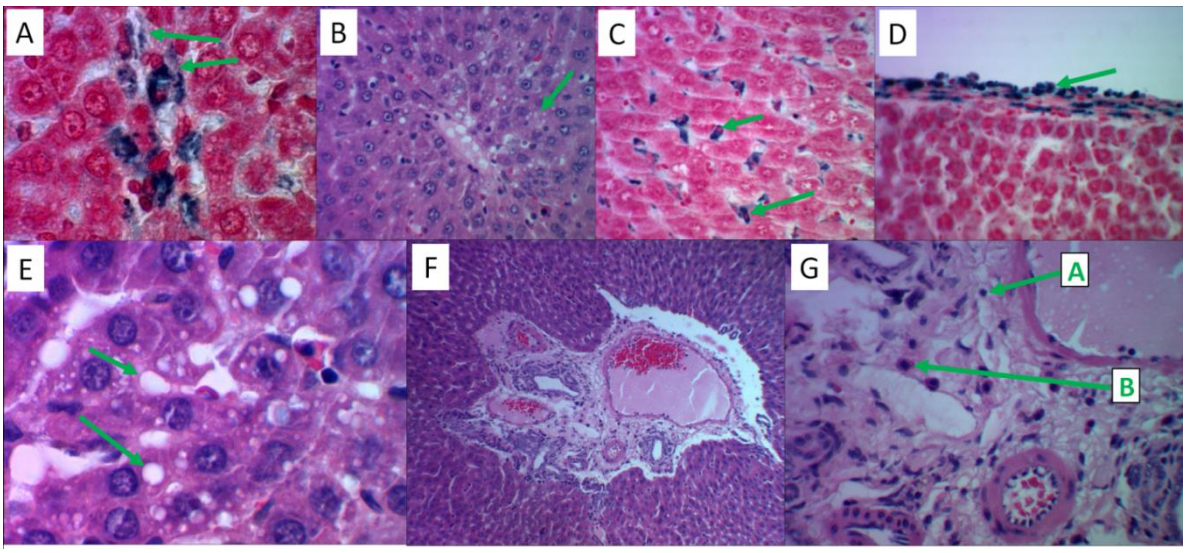

Figure 5. Histological analysis of liver tissues in the reproduction of the "iron sulfate + palm oil + fructose solution" model. Hematoxylin and eosin staining – slides B, E, F, G; Perls' reaction staining – slides A, C, D. Slides B, C, F – magnification x480, slides A, D, E, G – magnification x1200. A) Intracellular and extracellular deposition of Prussian blue granules on the periphery of the liver lobule. B) Fine-droplet obesity of hepatocytes in the center of the liver lobule. C) The cytoplasm of stellate reticuloendotheliocytes (Kupffer cells) is saturated with Prussian blue. D) Focal accumulation of Prussian blue in the liver capsule. E) Large-droplet obesity of hepatocytes in the center of the liver lobule. F) Inflammatory cell infiltration of the stroma of the portal tract. G) The infiltrate contains T-lymphocytes (marked with letter "A") and eosinophils ("B").Authors should discuss the results and how they can be interpreted from the perspective of previous studies and of the working hypotheses. The findings and their implications should be discussed in the broadest context possible. Future research directions may also be highlighted.

2.4.3. Model reproduction, the effects on kidneys

The study of histological sections of the renal cortical zone on the 12th day of the experiment showed the accumulation of small "iron grains" in the cytoplasm of nephrocytes of the proximal convoluted tubules, which was diffuse and focal. In 2 observations, the lumens of the distal convoluted tubules were obstructed by eosinophilic masses of insoluble carbohydrates and lipids, which indicated a violation of the glomerular filter. By the 41st day of the experiment, active excretion of iron-containing compounds was observed, which was confirmed by blue staining of urine in the lumens of the distal parts of the convoluted tubules. At the same time, nephrocytes of the distal tubules began to actively accumulate "iron grains" in the cytoplasm. Nephrocytes of the proximal tubules contained a few grains of the Prussian blue in the cytoplasm.

2.4.4. Model reproduction, the effects on brain and heart

When examining the brain by the 13th day of the experiment, focal accumulation of iron-containing substances in the perivascular space was observed against the background of moderately expressed perivascular and pericellular edema of the nervous tissue. No structural abnormalities of neurons were found. By the 41st day from the beginning of the experiment, single foci with lumps of Prussian blue remained in the nervous tissue of the cerebral hemispheres and cerebellum. In addition, activity of astrocytes was noted, in the cytoplasm of which small granules of iron-containing products were located.

Examination of the heart tissue of experimental animals showed the preservation of the parenchymatous and stromal-vascular elements of the myocardium (the 13th and 41st days). Minimal changes were found only in 2 observations in the form of small focal deposition of Prussian blue granules in the cytoplasm of cardiomyocytes.

 doi:10.20944/preprints202409.1645.v

2.4.5. Histological analysis of the effects of the MI treatment

After 41 days from the start of the experiment, centrilobular foci of fatty degeneration of hepatocytes were detected in the liver of laboratory animals (in 5 out of 6 cases), and quite small granules of Prussian blue were determined in the cytoplasm of individual hepatocytes (Figure 6A). The Perls reaction indicated the accumulation of iron-containing adducts in Kupffer cells and in the liver capsule (Figure 6B). In 4 observations, inflammatory cell infiltration of the stroma of the portal tracts with a predominance of eosinophils was noted (Figure 6C). According to histomorphometry data (number/percentage of Kupffer cells per field stained by Prussian blue) MI did not affect the iron accumulation by day 41 (MI: 25.2±3.5, model: 21.7±3.9).

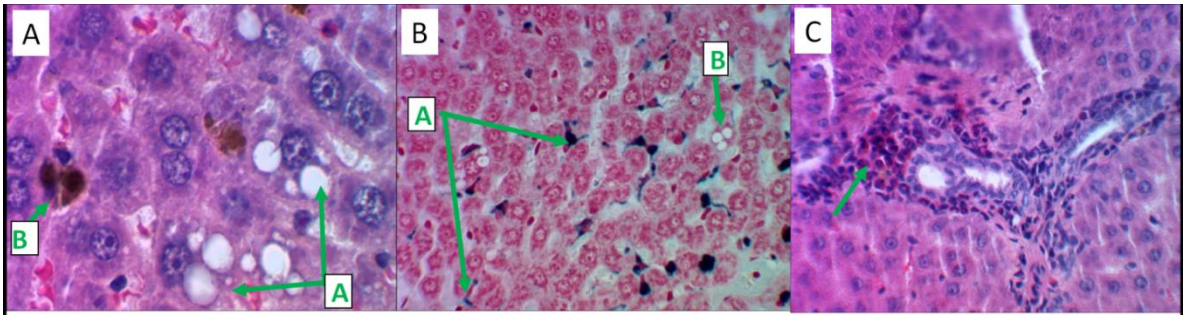

Figure 6. Histological analysis of MI effects on liver tissue. Hematoxylin and eosin staining – slides A, B; Perls reaction staining – slide B. Slides B, C – magnification x480, slide A – magnification x1200. A) Large-droplet obesity of hepatocytes in the centers of lobules (label "A"), iron-containing substrate in the cytoplasm of Kupffer cells (label "B"). B) Prussian blue in Kupffer cells, Disse space (label "A"), fatty degeneration of hepatocytes (label "B"). C) Predominance of eosinophilic leukocytes in the inflammatory infiltrate of the stroma of the portal tract.

When examining the kidneys, granules of Prussian blue were found in the cytoplasm of nephrocytes of the proximal convoluted tubules (Figure 7A), the contents of the lumens of the distal tubules are saturated with "iron grains" (Figure 7B). Chronic interstitial nephritis was detected in two observations (Figure 7C). At the same time, the Perls reaction did not reveal the presence of iron-containing products in the nervous tissue of the cerebral hemispheres and cerebellum (Figure 7D). In 3 of 6 observations, when conducting the Perls reaction in the myocardium, small accumulations of iron-containing granules were found in the cytoplasm of cardiomyocytes of the perivascular zone (Figure 7E).

 doi:10.20944/preprints202409.1645.v

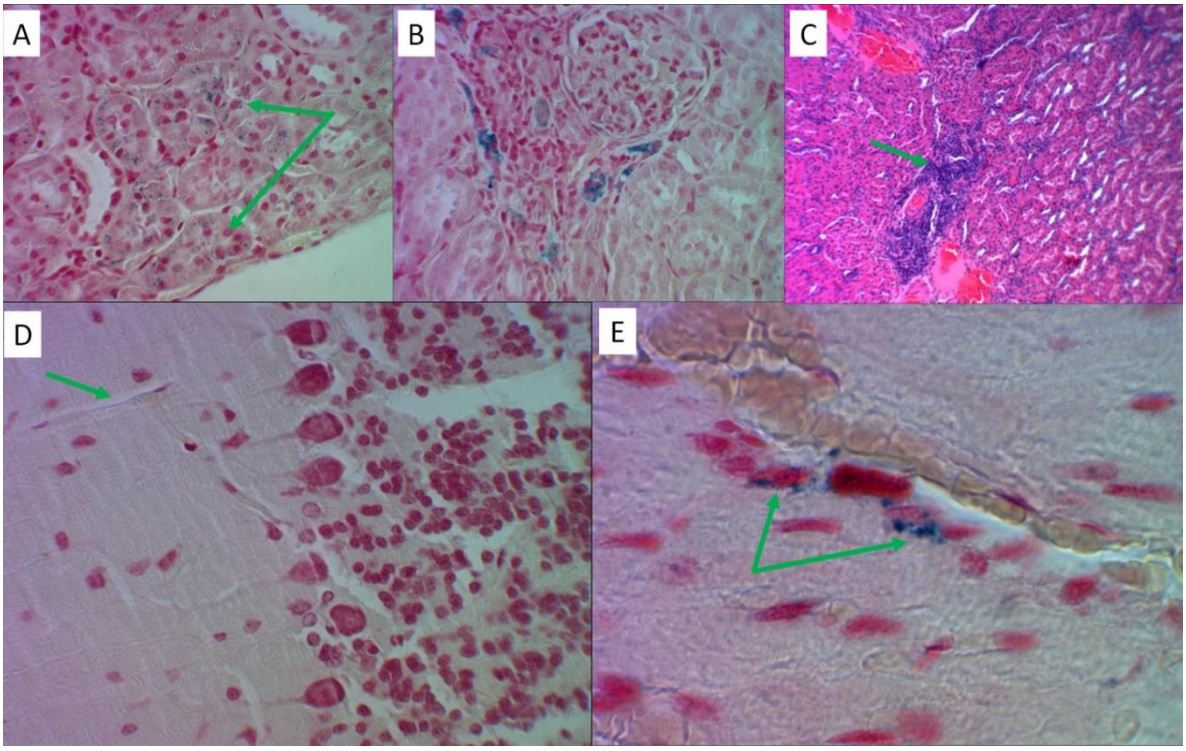

Figure 7. Histological analysis of MI effects on kidney, brain and myocardial tissues. Hematoxylin and eosin staining – slide C; Perls reaction staining – slides A, B, D, E. Slides A, B, D – magnification x480, slides C, E – magnification x1200. A) Prussian blue in proximal tubular nephrocytes. B) Iron-containing products in nephrocytes and in the lumens of distal tubules. C) Focal lymphocytic infiltration of the renal stroma. D) Moderate perivascular edema of the cerebellar nervous tissue in the absence of iron-containing products. E) Perivascular zone cardiomyocytes contain Prussian blue granules.

2.4.6. Histological analysis of the effects of lithium ascorbate

Perls reaction showed the presence of some Prussian blue staining in single stellate reticuloendotheliocytes and within liver capsule (Figure 8A). By day 41 no damage to hepatocytes was observed in the group on LiAsc; single lymphocytes were detected in the stroma of portal tracts, which correspond to an absence of a prominent inflammatory reaction of the liver (Figure 8B). Histomorphometry data (Kupffer cells stained by Prussian blue) confirmed that LiAsc greatly contributed to the decrease of the Prussian-blue-stained Kupffer cells (18.8±2.5, P=0.1 when compared with intact group).

In the study of the kidneys, small lumps of the Prussian-blue-stained particles were found in the cytoplasm of nephrocytes of the distal tubules in 4 cases (Figure 8C) while in the other two cases the kidneys were completely intact (no signs of staining for iron). In 2 cases, in the absence of circulatory disorders and structural abnormalities of neurons, with quite small lumps of Prussian blue were found in the perivascular space of the nervous tissue of the cerebral cortex (Figure 8D). Histological analysis of the myocardium did not reveal structural abnormalities of myocardial cardiomyocytes or the presence of any iron-containing products (Figure 8E). The results suggest that LiAsc can prevent the formation of stable iron-containing adducts (i.e., hemosiderin) in various organs – liver, kidneys, heart, brain.

 doi:10.20944/preprints202409.1645.v

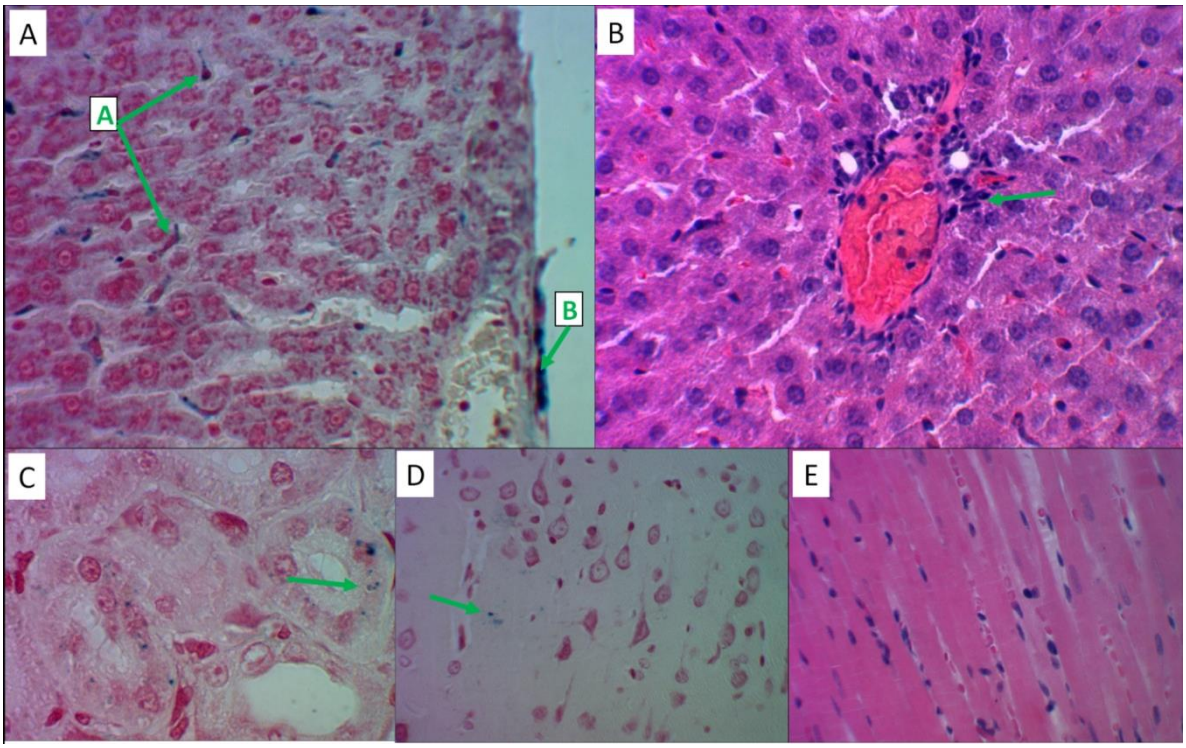

Figure 8. Histological analysis of the effects of lithium ascorbate. Hematoxylin and eosin staining – slides B, E; Perls reaction staining – slides A, C, D. Slides A, B, D - magnification x480, slides C, E - magnification x1200. A) An insignificant amount of iron-containing products in the cytoplasm of Kupffer cells (label "A"), liver capsule (label "B"). B) Single lymphocytes in the stroma of the portal tract. C) Grains of Prussian blue in nephrocytes of the distal convoluted tubules. D) Small lumps of Prussian blue in the perivascular space of the nervous tissue. E) Cardiomyocytes are uniformly stained, contractile fibers with transverse striation, capillary perfusion is preserved.

3. Discussion

The results of **chemoreactomic modeling** of hepatoprotection of several lithium salts and of MI indicated, at the very least, a possibility that LiAsc might show some hepatoprotective properties (protection against D-GalN-induced cytotoxicity, D-galactosamine-induced cytotoxicity, modeling in Zucker diabetic rats), that are comparable to a substance with known hepatoprotective properties (MI). At the same time, no such properties were predicted for lithium carbonate nor lithium comenate (data were not shown).

Analysis of the **normalized profiles of biochemical parameters** allowed us to obtain a more comprehensive picture of the differences in the effects of the studied approaches to iron overload therapy than using any individual parameters (AST/ALT, blood iron levels, etc.). We divided components of these profiles into three segments: iron metabolism parameters, general blood test parameters, and biochemical parameters of multiple organ dysfunction.

Among the **indicators of iron metabolism** both treatment with LiAsc and MI by day 41 resulted in a significant decrease in ferritin (MI: 173±52 μg/L, LiAsc: 203±4 μg/L), transferrin saturation (MI: 36±9%, LiAsc: 16±8%, all $P<0.00005$) and of serum iron (MI: 23±5 μmol/L, LiAsc: 13±4). Morphometrically determined number of Kupffer cells stained with Prussian blue was unaffected by MI and significantly reduced by LiAsc (18.8±2.5, $P=0.1$ when compared with intact group). This allows us to assume that *LiAsc is quite efficient in reducing the iron overload of the hepatic tissue*. This assumption was, actually, supported by the histological data.

Consideration of changes in the **general blood test parameters** allowed us to evaluate hematopoietic effects of the reproduction of the NAFLD model and of the pharmacotherapeutic agents applied. One of the main parameters of iron metabolism and hematopoiesis is the level of

 doi:10.20944/preprints202409.1645.v

hemoglobin in the blood. When reproducing the model, an observable decrease in the total number of red blood cells was noted (intact 8.7±0.8 trln cells/l, model day 13 7.4±1.2 trln/l). This may be due to the fact that iron/fat overload stimulates destruction of erythrocytes and/or shortens the red blood cell life cycle.

The acceleration of the erythrocyte life cycle (which implies, in particular, activation of hematopoiesis processes) under conditions of iron overload is also indicated by a *sharp increase in the reticulocyte* levels during the model reproduction. Recall that reticulocytes are young erythrocytes formed in the bone marrow, precursor cells of erythrocytes. The reticulocyte content in the blood reflects the state of the hematopoietic system (primarily erythropoiesis). All three indicators characterizing various aspects of the reticulocyte content in the blood (% of reticulocytes, reticulocyte content, reticulocyte fraction) were significantly increased during the model reproduction. MI did not have a significant effect on all the three parameters of reticulocytes (P>0.1) but LiAsc stimulated a decrease in total reticulocyte count (291±45 bln/L, P=0.0052) and reticulocyte fraction (51±6%, P=0.0275) towards the normal range on day 41 thus, probably, normalizing hemopoiesis towards the state of intact animals.

Biochemical **indicators of multiple organ dysfunction** characterized inflammation (white blood cells), thrombus formation (platelets) and the degree of cytolysis of the tissues (AST, ALT *etc*). One of the main signs of multiple organ dysfunction is an increase in proinflammatory and prothrombotic reactions of the body. In the present study, this corresponded to a significant increase in the levels of leukocytes (inflammation) and platelets (coagulation/aggregation of blood) when reproducing the NAFLD model with iron overload. Therapeutic interventions, on the contrary, contributed to a decrease in both leukocytes and platelets.

The state of the **liver function** is often characterized by levels of aspartate aminotransferase (AST), alanine aminotransferase (ALT), total serum protein, bilirubin (total, direct), vitamins B9 (folates) and vitamin B12 (cyanocobalamin). With damage to parenchyma of the liver, the levels of AST/ALT, bilirubin, vitamin B12 and folates, as a rule, increase (due to cytolysis of hepatocytes with the release of cell contents) while the levels of total protein - fall (due to deterioration of the biosynthetic function of the liver).

When reproducing the NAFLD model, the levels of AST, ALT, folates did increase, while the levels of total protein decreased. However, we observed an unusual dynamics of bilirubin levels (a decrease in total and direct bilirubin) and a decrease in vitamin B12 levels. In general, both LiAsc and MI contributed to the restoration of the values of these parameters towards the range of values characteristic for intact animals.

The enzymes AST and ALT are present in the highest concentrations in hepatocytes (also in cardiomyocytes and muscles). Normally, the levels/activity of AST/ALT in the blood are relatively low which prompts researchers and doctors to use AST and ALT as “liver function tests”. An increase in AST/ALT is indeed a characteristic feature of NAFLD, and a decrease in AST/ALT towards the reference range characterizes the effectiveness of an NAFLD therapy.

Reproducing the model resulted in a drastic increase in AST from 114.9±27.3 to 301.3±30.3 U/L (P<0.000001) on day 41. MI and LiAsc contributed to achieving AST levels similar to those in intact animals on day 41 (MI 94±35 U/L, P<0.000001; LiAsc 121.9±2.0 U/L, P=0.000013). Almost entirely similar picture was observed with ALT levels (see Results section). Changes in AST/ALT levels in groups 2–4 were consistent with changes in serum total protein levels (which represent a biomarker of biosynthetic function of liver). Both MI and LiAsc had a positive effect on liver biosynthetic function, promoting recovery of total protein levels by day 41 (MI 60.7±3.7 g/L, P=0.0001; LiAsc 52.5±1.0 g/L, P=0.01).

Vitamin B9 (folates) is a water-soluble vitamin required for the synthesis and methylation of DNA, the amino acids glycine and methionine. Measuring folate levels in the blood is commonly used to diagnose folate deficiency, which occurs due to (1) insufficient dietary intake (including consumption of thermally processed food), (2) decreased intestinal absorption of folates, (3) intake of drugs that impair absorption/metabolism of folates (estrogens, NSAIDs, cytostatic drugs, etc.). Causes of increased folate levels include intake of special folate-containing drugs or hepatocyte

 doi:10.20944/preprints202409.1645.v

cytolysis. Also, an increase in folates during model reproduction may be compensatory in nature: folates are important for cell division, including restoration of the pool of hepatocytes and erythrocytes. When reproducing the model, blood folate levels showed an upward trend (67.6±3.1 nmol/L, P=0.043). While MI had no significant effects on folates. LiAsc contributed to a decrease to the normal range (49.6±2.9 nmol/L, P<0.000005 when compared with model at day 41, P>0.1 when compared with intact) which is yet another indication of the hepatoprotective properties of LiAsc (lower cytolysis).

Folate level usually correlate with vitamin B12 levels (since folate and vitamin B12 deficiencies often coexist). However, when reproducing the present model, the above-mentioned increase in folate levels was combined with a decrease in blood vitamin B12 levels (intact 264.5±58.1 pg/mL, model, day 13 190.5±7.1 pg/mL, P=0.013) which indicated the development of a deficiency. MI did not affect B12 levels (P=0.096) but LiAsc promoted normalization of vitamin B12 levels, to levels significantly higher than in intact animals (day 41: 325.3±23.1 pg/mL, P<0.00001 compared with model on day 41, P<0.001 compared with intact).

The main reasons for a decrease in vitamin B12 levels in the blood are insufficient intake, inflammatory and other bowel diseases, absorption disorders, including against the background of liver and kidney diseases or taking a number of drugs (colchicine, anticonvulsants, antibiotics reduce the concentration of B12). Since renal dysfunction was indeed observed in the model (see above), this is the most likely factor determining the decrease in vitamin B12 levels.

A statistically significant restoration of the concentration of vitamin B12 in the blood to the values of intact animals represent rather unexpected effect of lithium ascorbate. In the pharmacology of micronutrients, the so-called "Thérèse Turuan phenomenon" is known, in which the intake of one or another vitamin helps to improve the supply of other vitamins to the body. This effect may be due to the direct effects of the lithium ion on target proteins of the proteome [18] or might be an indirect consequence of the hepatoprotective effect of LiAsc.

Despite the fact that hepatocyte cytolysis (reflected by an increase in AST, ALT, vitamin B9, bilirubin and a decrease in total protein) is characteristic of liver pathology, when reproducing the present model, total bilirubin levels significantly decreased (intact 5.9±0.6 μmol/L, model, day 13 1.5±1.1 μmol/L, P=0.000016), with an insignificant increase by day 41 (2.1±1.4 μmol/L). Recall that bilirubin and its fractions (total, direct, indirect) are metabolites of heme breakdown (a component of the hemoglobin protein). Therefore, the levels of various fractions of bilirubin increase with activation of red blood cell destruction, dysfunction of the liver and biliary tract, accompanying a wide variety of pathologies (hemolytic anemia, myocardial infarction, sepsis, viral hepatitis, biliary atresia, alcoholic liver disease, NAFLD, etc.).

Causes of decreased total/direct bilirubin are much rarer and include renal failure, acute leukemia, tuberculosis, anemias of various origins, including those resulting from taking various drugs (barbiturates, valproates, caffeine, corticosteroids, penicillin, sulfonamides, etc.). In our view, the most likely explanation for the decrease in bilirubin levels when reproducing the NAFLD model with iron overload was renal dysfunction (as indicated by decrease in creatinine and GFR levels). Only MI contributed to a significant restoration of total bilirubin levels on day 41 (5.3±1.2 μmol/L, P=0.0011), with no significant effect for lithium ascorbate (1.9±0.7 μmol/L).

Histological confirmations of the model and of the effects of the substances indicated progression from normality (as evidenced by histology of the intact group) to iron/lipid overload after reproducing the NAFLD model. Liver samples indicated progression of fatty degeneration of hepatocytes, inflammatory cell infiltrate (T-lymphocytes, eosinophils, intracellular and extracellular deposition of Prussian blue granules on the periphery of the liver lobule. Nephrocytes of the distal tubules began to actively accumulate "iron grains" in the cytoplasm; a focal accumulation of iron-containing substances was noticed in the perivascular space of neural tissue. In general, the developed complex model of secondary hemochromatosis and liver steatosis had reliable morphological confirmation.

When reproducing the model, structural changes in the liver, kidneys, brain and myocardium at the microscopic level were established, characteristic of multiple organ pathology. *In the liver,*

 doi:10.20944/preprints202409.1645.v

accumulation of iron-containing products (hemosiderin) in the cytoplasm of hepatocytes and in the Disse space of the periportal zone of the liver lobule was observed. Macrophage activity of stellate reticuloendotheliocytes (Kupffer cells) was revealed with a tendency to an increase in the level of phagocytosis of iron-containing products by the 41st day of the experiment. Fatty degeneration of hepatocytes (as the main morphological criterion of steatosis) was diffuse-focal in nature with localization in the centers of liver lobules and was expressed by small-droplet obesity of hepatocytes on the 13th day of the experiment, with large-droplet obesity by the 41st day. The presence of inflammatory cell infiltrate with eosinophils in the stroma of portal tracts indicates the development of hepatitis.

After the model was reproduced (day 13), infiltration of iron-containing products into the cytoplasm of *nephrocytes* along the entire length of the tubules was established in the *kidneys,* without significant blood flow disorders and inflammatory reaction. By the 41st day of the experiment, excretion and reabsorption of iron was noted, which led to an overload of iron-containing products in the nephrocytes of the proximal and distal convoluted tubules.

In the brain and myocardium, the content of "iron grains" was minimal and was observed as focal areas of accumulation of small lumps of Prussian blue in the absence of morphological signs of any toxic effect on the parenchymatous elements of these organs. Possible reasons for the minimal effect on the brain include short periods after the reproduction of the model and the filtering role of the blood-brain barrier. In the case of the myocardium, the minimal amount of iron deposits is most likely associated with the constant motor activity of this organ and with the high number of mitochondria in cardiomyocytes (which accelerates the cell detoxification cycle).

Histological studies also confirmed the results of biochemical tests in the sense that LiAsc apparently had “anti-hemosiderin” properties as evidenced by morphometrics with Kuppfer cells and by quite a number of positive effects on the state of tissues of liver, brain and kidneys, including lowering of inflammation, lipid hyperaccumulation and iron overload of the tissues.

It also seems proper to discuss the **putative molecular mechanisms of hepatoprotective action of the LiAsc** which are related to the molecular-biological properties of the ascorbate anion and of the lithium ion. The hepatoprotective properties of *ascorbic acid, ascorbates and of a few of the ascorbic acid derivatives* [19,20] are known, especially when used in combinations with other substances of hepatoprotective quality: alpha-lipoic acid, polyphenol silymarin [21], anti-diabetic drug metformin [22], vitamin PP (nicotinamide) [23] *etc*.

Possible mechanisms of the hepatoprotective action of ascorbate might included the obvious antioxidant effect [24] (which includes restoration of the levels of glutathione GSH and of antioxidant enzymes SOD-1/2, CAT [25]), inhibition of sulfatase-2 and reduced expression of pro-inflammatory protein factor NFkB, CRP, TNF-a, IL-1b, IL-6 [26], reduction of expression of pro-apoptotic caspase-3, of pro-fibrotic TGF-beta and collagen-I genes [27]. Ascorbic acid supplementation in such cases is done in quite high doses. For example, 1.5 mg/ml in the drinking water to mice is roughly equivalent to 225 mg/kg/day does which, in turn, corresponds to intake of 1000-2000 mg/day of vitamin C by an adult human [28].

On the contrary, studies of *lithium carbonate* (done in high doses, corresponding to intake of 1-10 g/day of Li_2CO_3 by human patients) usually indicate hepatic injury as a typical consequence. Rather, the effects of various substances against Li_2CO_3-induced hepatotoxicity are investigated [29,30]. However, results of at least one clinical study indicate that more discrete usage even of relatively toxic Li_2CO_3 can, actually, reduce hepatic injury or leukopenia in patients with Graves' disease [31].

Potential mechanism of the *hepatoprotective action of lithium ion* involves, most likely, the inhibition of the glycogen synthase kinase-3 beta (GSK-3β) target protein. It is common knowledge that lithium ion can specifically bind to and inhibit GSK-3β. The experimental evidence available allows us to state that inhibition of GSK-3β can favorably influence hepatic function. For example, one of the histologically confirmed toxic effects of lead acetate includes significantly reduced phosphorylation of the liver GSK-3β. On the contrary, supplementation of rats with hepatoprotective L-carnitine resulted in an increase in phosphorylation of the liver GSK-3β. It is well known that

 doi:10.20944/preprints202409.1645.v

phosphorylation of serine-9 in GSK-3β (serine-21 in GSK-3*α*) results in inhibition of GSK-3 kinases [32], thus inhibition of GSK-3β would have a benign influence on the liver.

4. Materials and Methods

The complex of studies reported here included an *in silico* chemoreactomic modeling of several lithium salts, synthesis of the lithium salt(s), development and histological confirmation of the *in vivo* rat model of NAFLD with iron overload and approbation of the effects of LiAsc and of MI on the NFALD model.

Chemoreactomic modeling of hepatoprotective effects of substances. As in our previous paper [1] before trying any actual experimental studies we modeled putative hepatoprotective properties of LiAsc and of several other lithium salts using the chemoreactomic approach to the analysis of the "structure-property" problem of organic molecules. The approach represents a relatively new direction of application of artificial intelligence (machine learning) systems in the field of post-genomic pharmacology. The rigorous mathematical methodology based on the theory of topological data analysis [33] and the algorithms that were realized within an original proprietary software developed by the authors that was previously described [34] and extensively tested [35]. The training of the algorithms was carried out on the basis of the data on structure and properties of the molecules presented in the PubChem database for which hepatoprotective properties were found. The resulting train/test subset of PubChem included the data for 3423 molecules for which 486 hepatoprotective activities were determined experimentally (as documented in PubChem). The algorithms and software developed were realized within the framework of the topological and metrical theories of the analysis of complex data with highly heterogeneous features [34,35]; additional information about the algorithms and their testing is presented in the internet at web sites www.chemoinformatics.ru and www.pharmacoinformatics.ru.

Substances used. The synthesis of the organic salts was based on the classical reaction of neutralization carried out with the organic acids and the lithium carbonate as described in [1]. The synthesis of LiAsc was carried out in accordance with the equation of the reaction of neutralization $2C_6H_8O_6 + Li_2CO_3 = 2C_6H_7O_6Li + H_2O + CO_2\uparrow$ from L-Ascorbic acid ($C_6H_8O_6$, Sigma-Aldrich, A5960, BioXtra, ≥99.0%) and lithium carbonate (Li_2CO_3, Merck, 1.05671.1000, certificates Ph Eur, BP, USP). Synthesis of sodium ascorbate (used in a preliminary comparative study) was performed similarly from sodium carbonate (Na_2CO_3, Merck, 1.06392.1000, grade ISO-1). Myoinositol was also of pharmaceutical grade ($C_6H_{12}O_6$, Merck, 1.04731.1000, certificates Ph Eur, FCC, NF).

Animal studies. During the animal studies, the animals were kept under standard conditions in accordance with Directive 2010/63/EU of the European Parliament and of the Council of the European Union of 22 September 2010 concerning the protection of animals used in scientific studies [36]. Indoor air control in compliance with environmental parameters (temperature 18-26 °C, humidity 46-65%). The rats were kept in standard plastic cages with a bedding, the cages were covered with steel lattice covers with a stern recess. Floor area per animal met regulatory standards. The animals were fed in accordance with Directive 2010/63/EU. The animals were given water *ad libitum*. The water was purified and normalized for organoleptic properties, in terms of pH, dry residue, reducing substances, carbon dioxide, nitrates and nitrites, ammonia, chlorides, sulfates, calcium and heavy metals in standard drinkers with steel spout lids. A 12-hour lighting cycle was maintained in the animal housing rooms. Environmental conditions were monitored using a Testo combined meter (manufactured by TestoAG, Germany) and recorded in a corresponding log. For acclimatization, laboratory animals were kept individually in cages for 5 days before the start of the study. During this period, the animals' clinical condition was monitored daily by visual inspection. Animals with deviations detected during the inspection were not included in the experimental groups.

The development of the iron overload NAFLD model was based on the NAFLD model induced by palm oil [5]. The development of the NAFLD model with multiple organ pathology and iron overload and testing of the effects of LiAsc therapy were carried out on 30 white male rats weighing 300-400 g. The animals were divided into 4 groups. At the beginning of the experiment, the animals were distributed into groups so that the individual body weight did not deviate from the average

 doi:10.20944/preprints202409.1645.v

body weight for the group by more than 20%. Weighing was carried out on electronic scales for weighing rats/mice (manufactured by Cas Corporation, Russia).

The first group (n=6) was an intact control (on a normal diet and drinking pure drinking water). In the second (n=12), third, and fourth (n=6) groups of animals, the model of liver iron overload was reproduced under conditions of adding saturated fats and fructose to the diet. To reproduce the model, chemically pure divalent iron sulfate (manufactured by JSC LenReaktiv, passport No. 070051-81, Russia) was administered intraperitoneally to the animals at a dose of 50 mg/kg/day for 12 days. At the same time, a solid fraction of palm oil (CandleM , Indonesia) was added to the diet at a dose of 30 g/kg/day. A fructose solution (LLC Sladkiy Mir Company, TU 10.86.10-027-72315488-2019. Batch 210723, Russia) at a dose of 1 g/kg/day was used instead of drinking water for 12 days.

On the 13th day of the study, animals of the first and of the second groups were anesthetized, blood was collected for biochemical testing and autopsy material (liver, kidneys, brain, heart) was collected for pathohistological testing. Animals were withdrawn from the experiment by achieving anesthetic death using the drug Zoletil.

Exploring different approaches to therapy was carried out from the 13th day of the study. The third group (n=6) received LiAsc (manufactured by Normofarm LLC, Russia) at a dose of 30 mg/kg/day *per os* for 4 weeks. The fourth group received myoinositol (400 mg/kg/day *per os*) for 4 weeks. On the 41st day of the study, the animals of the second, third, and fourth groups (n=6) were anesthetized, blood was collected for biochemical analysis, and autopsy material (liver, kidneys, brain, heart) was collected for histopathological examination.

The animals were observed daily; their general condition, appetite, behavioral characteristics, intensity and nature of motor activity, frequency and depth of respiratory movements, condition of hair and skin, tail position, amount and consistency of feces were recorded. The values of more than 20 biochemical parameters were determined in the blood (Table 2) using the methods described in Table 3.

Table 2. Biochemical parameters (indicators) measured in this work

Abbreviation	Biochemical indicator
Ferritin	Ferritin, mcg/l
Sat.transferrin	Transferrin iron saturation coefficient, %
Serum Iron	Serum iron, μmol/l
Reticulocytes, %	Reticulocytes, %
Reticulocytes, abs.	Reticulocytes, bln/l
Frac. reticulocytes,%	Reticulocyte fraction, %
Leukocytes, abs.	Leukocytes, bln/l
Erythrocytes, abs.	Erythrocytes, trln/l
Hemoglobin	Hemoglobin, g/l
Hematocrit, %	Hematocrit, %
V-erythrocyte	Mean corpuscular volume, fL
Hemoglobin-erythrocyte	Average hemoglobin content in erythrocytes, pg
Conc.hemoglobin erythrocytes	Average hemoglobin concentration in red blood cells, g/l
Platelets, abs.	Platelets, bln/l
Ind. Mentzer	Mentzer Index
Ind. Sirdah	Sirdah Index
Vitamin B9	Vitamin B9 (folic acid), nmol/l
Tot.protein	Total protein in serum, g/l

 doi:10.20944/preprints202409.1645.v

AST	Aspartate aminotransferase, U/L
ALT	Alanine aminotransferase, U/L
Creatinine	Serum creatinine, μmol/l
GFR	Glomerular filtration rate, ml/min/1.73m^2
Tot.bilirubin	Total bilirubin, μmol/l
Dir.bilirubin	Direct bilirubin, μmol/l
Vitamin B12	Vitamin B12 (cyanocobalamin), pg/ml
Kupffer cells	Kupffer cells, which contain Prussian blue in their cytoplasm (after Perls reaction)

Table 3. Methods and equipment used to measure biochemical indicators.

Indicator	**Method**	**Equipment**
Ferritin	Immunoturbidimetry	Cobas 6000, Roche Diagnostics, Switzerland
Transferrin	Immunoturbidimetry	Cobas 6000, Roche Diagnostics, Switzerland
Serum iron	Colorimetric photometric method	Cobas 6000, Roche Diagnostics, Switzerland
Reticulocytes	Flow cytometry	BC-6200, Mindray, China
Leukocytes Erythrocytes Hemoglobin Hematocrit Mean corpuscular volume Average hemoglobin content in red blood cells Average hemoglobin concentration in red blood cells Platelets	Conductometric method based on SLS (sodium lauryl sulfate), flow cytometry	BC-6200, Mindray, China
Total protein Total bilirubin Direct bilirubin	Colorimetric photometric method	Cobas 6000, Roche Diagnostics, Switzerland
Aspartate aminotransferase (AST)	UV kinetic test	Cobas 6000, Roche Diagnostics, Switzerland

 doi:10.20944/preprints202409.1645.v

Alanine aminotransferase (ALT)		
Serum creatinine (with GFR determination)	Jaffe's "kinetic" method	Cobas 6000, Roche Diagnostics, Switzerland
Vitamin B_{12}	Immunochemiluminescent assay	Cobas 6000, Roche Diagnostics, Switzerland
Vitamin B_9	Competitive solid-phase chemiluminescent enzyme immunoassay	Cobas 6000, Roche Diagnostics, Switzerland

Histopathohistological studies. Material for histological examination was obtained during autopsy of experimental animals. The brain was removed entirely by craniotomy and fixed in 10% neutral formalin solution; after 24 hours, the precentral gyrus zone of the forebrain, cerebellum, and brainstem were isolated using frontal incisions. After evisceration, the liver, heart, and kidneys were fixed in 10% neutral formalin solution. After 24 hours, the organs were dissected, fragments of the left ventricular myocardium, right and left lobes of the liver, and cortical sections of the right and left kidneys were isolated and re-fixed. After secondary fixation and washing of the material, dehydration of the brain, liver, and kidney tissues was performed using 99% isopropyl alcohol. The pieces were then embedded in paraffin and histological sections 5-6 μm thick prepared on sliding microtome "Microm" and were stained with hematoxylin and eosin. Duplicates of the sections were stained according to Perls using a set of reagents from the Biovitrum (Russia) to detect trivalent iron in the tissues. In the case of the presence of an excess trivalent ionic iron in tissues the result of the Perls' reaction should be the formation of the blue-colored salt – the Prussian blue (according to the equation of the chemical reaction $Fe^{III}Cl_3 + K_4[Fe^{II}(CN)_6] \rightarrow KFe^{III}[Fe^{II}(CN)_6] + 3KCl$).

The qualitative assessment of pathological changes in the tissues took into account the degree of circulatory disorder, the presence and localization of Prussian blue, the characteristics of the inflammatory response, and structural changes in parenchymatous elements. Micrographs were obtained using a research microscope "Micros" MS-200 with a digital ocular camera DCM 900 (UK). Quantitative assessment of the iron overload through morphometric analysis was performed on the liver samples (item "Kupffer cells" in Table 1) by counting the average number of Kupffer cells containing Prussian blue in their cytoplasm per field of view.

Statistical analysis. The results were processed using the Excel 2013 and Statistica 10.0 (USA) software packages. The significance of differences between groups was determined by a nonparametric U-test, the Wilcoxon – Mann – Whitney test.

To construct profile diagrams of the biochemical parameters listed in Table 1, the cumulative empirical distribution functions (CDF) of each of the studied parameters were first calculated. Recall that the CDF F(X) of the values of parameter X is a function in the range of values [0…1], on the graph of which the values of parameter X (for example, ferritin levels) in all experiments are plotted along the X axis, and the probability that the value of X is less than a given value is plotted along the Y axis. For example, if the maximum value of ferritin in the blood collected during the experiments was 500 μg/L, then the probability that an arbitrary value ferritin less than 500 equals to 1 (i.e. all observed values were less than 500 μg/L).

Then, the values of each X parameter in their generally accepted units of measurement (e.g., μg/L for ferritin) were replaced by the values of the CDF F(X) in dimensionless units in the range of values [0...1]. Using the CDF values instead of the original values of the parameters allows for a clear comparison of the effects of various therapeutic interventions on a single scale of values in the range [0...1]. At the same time, the absolute values of the parameters studied may differ by 1-2 orders of

 doi:10.20944/preprints202409.1645.v

magnitude. For example, the values of ferritin lie in the range of 72-277 μg/L, and total bilirubin - in the range of 0.3-6.7 μmol/L. Obviously, a diagram with such significant differences in the orders of magnitude of the parameter values will not be informative nor visually acceptable.

5. Conclusions

This study reports hepatoprotective properties of the neuroprotective salt lithium ascorbate tested on a model of non-alcoholic fatty liver disease with iron overload. In clinical practice, NAFLD originates as a result of dietary disorders (excess fats, carbohydrates, xenobiotics, micronutrient deficiencies, etc.) and, being aggravated by iron overload, quickly progresses to multi-organ pathology (damage not only to the liver, but also to kidneys, heart, brain and, probably, other organs). The model of NAFLD proposed in this paper was apparently alleviated by quite unexpected a substance – neuroprotector LiAsc. A complex of similarities and differences in the biochemical and histological differences in the effectiveness of LiAsc and hepatoprotective myoinositol was elucidated. Of particular interest is to notice that LiAsc can reduce iron overload of the Kupffer cells of the liver – an action which was not observed for MI. Additional hepatoprotective 'fringe benefits' of a neuroprotector substance do not only indicated a favorable safety profile but also might be useful in treatment of neurological patients that also have a tendency to iron overload and liver damage (which is the case, for instance, of hepatic encephalopathy).

6. Patents

Several part of this work resulted earlier in patents (1) Bogacheva TE, Dibrova EA, Gromova OA, Grishina TR, Kalacheva AG, Demidov VI, Torshin IY, Tomilova IK. Method for assessing the effectiveness of the drug "Laennec" in creating a pharmacological model of steatohepatosis in experimental animals. Patent application RU2023102563 dated February 3, 2023. PATENT RU 2811886 and (2) Gromova OA, Rastashanskiy VV, Ostrenko KS. Use of lithium ascorbate to prevent and treat alcoholism and alcohol intoxication, Grant Date 11.01.2022, Patent US20200147128

Supplementary Materials: The following supporting information can be downloaded at: www.mdpi.com/xxx/s1, Figure S1: title; Table S1: title; Video S1: title.

Author Contributions: Conceptualization, I.T., O.G.,; methodology, all authors; software, I.T.; validation, I.T., O.G.; formal analysis, I.T.; data collection and investigation, all authors; resources, O.G., T.B.; data curation, I.T., O.G.; writing—original draft preparation, I.T.; writing—review and editing, O.G.; visualization, I.T.; supervision, O.G.; project administration, O.G. All authors have read and agreed to the published version of the manuscript.

Funding: This research received no external funding.

Institutional Review Board Statement: The study was conducted according to the guidelines of the Declaration of Helsinki, and approved by the Institutional Review Board of Ivanovo State Medical Academy (protocol code 3, 11 November 2023).

Data Availability Statement: The data are available upon reasonable request.

Acknowledgments: In this section, you can acknowledge any support given which is not covered by the author contribution or funding sections. This may include administrative and technical support, or donations in kind (e.g., materials used for experiments).

Conflicts of Interest: The authors declare no conflict of interest.

References

1. Torshin, I.Y.; Gromova, O.A.; Ostrenko, K.S.; Filimonova, M.V.; Gogoleva, I.V.; Demidov, V.I.; Kalacheva, A.G. Lithium Ascorbate as a Promising Neuroprotector: Fundamental and Experimental Studies of an Organic Lithium Salt. *Molecules* **2022**, 27, 2253. https://doi.org/10.3390/molecules27072253
2. Torshin, I.Yu.; Sardaryan, I.S.; Gromova, O.A.; Rastashansky, V.A.; Fedotova, L.E. Chemoreactome modeling the effects of anions of lithium salts ascorbate, nicotinate, hydroxybutyrate komenata and lithium

carbonate. *Pharmacokinetics and Pharmacodynamics*. **2016**;(3):47-57. (In Russ.) https://www.pharmacokinetica.ru/jour/article/view/185

3. Nazarenko, O.A.; Demidov, V.I.; Gromova, O.A.; Aleksakhina, E.L.; Torshin, I.Yu. Comparative study of the neuroprotective activity of lithium compounds and their effect on the course of experimental alloxan diabetes mellitus in rats. *Pharmacokinetics and Pharmacodynamics*. **2020**;(3):40–47. DOI: 10.37489/2587-7836-2020-3-40-47
4. Torshin, I.Yu.; Gromova, O.A.; Lazebnik, L.B. Chemomicrobiome analysis of lithium ascorbate and other organic lithium salts. *Experimental and Clinical Gastroenterology*. **2022**;(9):95-104. (In Russ.) https://doi.org/10.31146/1682-8658-ecg-205-9-95-104
5. Bogacheva, T. E.; Kalacheva, A.G.; Gromova, O.A.; Torshin, I.Yu.; Grishina, T.R.; Demidov, V.I. Study of the effectiveness of the drug Laennec in liver damage by palm oil in rats. *Pharmacokinetics and Pharmacodynamics*. – **2023** (4):23-32.
6. Zhuo, Z.; Fan, S.; Hu K.; Huang, D.; Feng, D. Analysis of digital profiling of duodenal transcriptome gene expression in SD rats injected with iron sulfate or iron glycine chelate through a probe. *Sci Rep*. **2016** Nov 30;6:37923. DOI: 10.1038/srep37923. PMID: 27901057; PMCID: PMC5128800.
7. Luo, G.; Xiang, L.; Xiao, L. Acetyl-CoA Deficiency Is Involved in the Regulation of Iron Overload on Lipid Metabolism in Apolipoprotein E Knockout Mice. *Molecules*. **2022** Aug 4;27(15):4966. doi: 10.3390/molecules27154966. PMID: 35956917
8. Hilton, S.; Sabaratnam, R.; Drakesmith, H.; Karpe, F. Metabolism of iron, glucose and fats and obesity: the relationship. *Int J Obes* (London). **2023** Jul; 47(7):554-563. DOI: 10.1038/s41366-023-01299-0 PMID: 37029208; PMCID: PMC10299911.
9. Jensen, T.; Abdelmalek, M.F.; Sullivan, S.; Nadeau, K.J.; Green, M.; Ronkal, S.; Nakagawa, T.; Kuwabara, M.; Sato, Y.; Kang, D.H.; Tolan, D.R.; Sanchez-Losada, L.G.; Rosen, H.R.; Lanaspa, M.A.; Dil, A.M.; Johnson, R.J. Fructose and sugar: the main mediators of non-alcoholic fatty liver disease. *J Hepatol*. May **2018**; 68(5):1063-1075. DOI: 10.1016/j.jhep.2018.01.019. Epub 2018 February 2. PMID: 29408694; PMCID: PMC5893377.
10. Ma, J.; Sloan, M.; Fox, KS, Hoffmann, W.; Smith, SE, Salzman, E.; Rogers, G.T.; Jacques, F.; McCown, N.M. Consumption of sugar-sweetened beverages is associated with the breakdown of abdominal fat in healthy adults. *J Nutr*. August **2014**; 144(8):1283-90. DOI: 10.3945/jn.113.188599. Epub 2014 June 18. PMID: 24944282; PMCID: PMC4093984.
11. Di Stefano, J.K. Fructose-mediated effect on gene expression and epigenetic mechanisms associated with the pathogenesis of NAFLD. *Cell Mol Life Sci*. **2020** June; 77(11):2079–2090. DOI: 10.1007/s00018-019-03390-0. PMID: 31760464; PMCID: PMC7440926.
12. Vos, M.B.; Lavin, J.E. Dietary fructose in non-alcoholic fatty liver disease. *Hepatology*. June **2013**; 57(6):2525-31. DOI: 10.1002/hep.26299. Epub 2013 May 1. PMID: 23390127.
13. Kanerva, N.; Sandboge, S.; Kaartinen, N.E.; Mianniste, S.; Eriksson, J.G. Higher consumption of fructose is inversely proportional to the risk of non-alcoholic golic fatty liver disease in elderly Finns 1-4 years. *American Journal of Clinical Nutrition*. **2014**;100:1133-1141. https://doi.org/10.3945/ajcn.114.086074
14. Ma, J.; Fox, K.S.; Jacques, F.; Speliotes, E.K.; Hoffmann, W.; Smith, S.E.; Saltzman, E.; McKeown, N.M. Sugar-rage, diet, and fatty liver disease in the cohorts of the Framingham Heart Study. *Hepatological Journal*. **2015**; 63(2):462-469. https :// doi . org /10.1016/ j . jhep.2015.03.032
15. Sheptulina, A.F.; Golubeva, Yu.A.; Drapkina, O.M. Fructose consumption as a risk factor for metabolic syndrome and nonalcoholic fatty liver disease. *Russian Journal of Evidence-Based Gastroenterology*. **2023**;12(1):85 92. (In Russ.). doi.org/10.17116/dokgastro.202312011851
16. Limanova, O.A.; Gromova, O.A.; Torshin, I.Yu.; Gromov, A.N.; Grishina, T.R. Systematic analysis of molecular mechanisms and physiological effects of myo-inositol: findings of molecular biology and clinical medicine. *Effektivnaja farmakoterapija. Akusherstvo*. **2012** 3(28):4-12.https://umedp.ru/articles/sistematicheskiy_analiz_molekulyarnofiziologicheskikh_effektov_mioinozitola_dannye_molekulyarnoy_bio.html
17. Gromova, O.A.; Torshin, I.Y.; Uvarova, E.V. Systematic analysis of the biological roles and pharmacological properties of D-chiro-inositol. *Gynecology*. - **2020**. - Vol. 22. - No. 3. - P. 21-28. doi: 10.26442/20795696.2020.3.200210.

18. Torshin, I.Yu.; Gromova, O.A.; Mayorova, L.A.; Volkov, A.Yu. Targeted proteins involved in the neuroprotective effects of lithium citrate. *Neurology, neuropsychiatry, psychosomatics*. **2017**;9(1):78–83. DOI: http://dx.doi.org/10.14412/2074-2711-2017-1-78-83
19. Vyshtakalyuk, A.B.; Nazarov, N.G.; Zobov, V.V.; Abdulkhakov, S.R.; Minnekhanova, O.A.; Semenov, V.E.; Galyametdinova, I.V.; Cherepnev, G.V.; Reznik, V.S. Evaluation of the Hepatoprotective Effect of L-Ascorbate 1-(2-Hydroxyethyl)-4,6-Dimethyl-1,2-Dihydropyrimidine-2-One Upon Exposure to Carbon Tetrachloride.*Bull Exp Biol Med*. **2017** Jan;162(3):340-342. doi:10.1007/s10517-017-3610-8. Epub 2017 Jan 14. PMID: 28091907
20. Mitra, A.; Kulkarni, A.P.; Ravikumar, V.C.; Bourcier, D.R. Effect of ascorbic acid esters on hepatic glutathione levels in mice treated with a hepatotoxic dose of acetaminophen.*J Biochem Toxicol*. **1991**;6(2):93-100. doi: 10.1002/jbt.2570060203. PMID: 1941904
21. Abdulrazzaq, A.M.; Badr, M.; Gammoh, O.; Abu Khalil, A.A.; Ghanim, B.Y.; Alhussainy, T.M.; Qinna, N.A. Hepatoprotective Actions of Ascorbic Acid, Alpha Lipoic Acid and Silymarin or Their Combination Against Acetaminophen-Induced Hepatotoxicity in Rats.*Medicina (Kaunas)*. **2019** May 21;55(5):181. doi: 10.3390/medicina55050181. PMID: 31117289
22. Adeneye, A.A.; Benebo, A.S. Oral metformin-ascorbic acid co-administration ameliorates alcohol-induced hepatotoxicity in rats. *Nig J Hosp Med*. **2007** Oct-Dec;17(4):155-9. doi: 10.4314/nqjhm.v17i4.12698. PMID: 18320763
23. Abd-Allah, H.; Nasr, M.; Ahmed-Farid, O.A.; Ibrahim, B.M.; Bakeer, R.M.; Ahmed, R.F. Nicotinamide and ascorbic acid nanoparticles against the hepatic insult induced in rats by high fat high fructose diet: A comparative study. *Life Sci*. **2020** Dec 15;263:118540. doi: 10.1016/j.lfs.2020.118540. Epub 2020 Oct 6. PMID: 33035588
24. Bispo, V.S.; Dantas, L.S.; Chaves, A.B. Filho, Pinto, I.F.D.; Silva, R.P.D.; Otsuka, F.A.M.; Santos, R.B.; Santos, A.C.; Trindade, D.J.; Matos, H.R. Reduction of the DNA damage, Hepatoprotective Effect and Antioxidant Potential of the Coconut Water, ascorbic and Caffeic Acids in Oxidative Stress Mediated by Ethanol. *An Acad Bras Cienc*. **2017** Apr-Jun;89(2):1095-1109. doi: 10.1590/0001-3765201720160581. Epub 2017 May 15. PMID: 28513780
25. Banerjee, P.; Bhattacharyya, S.S.; Bhattacharjee, N.; Pathak, S.; Boujedaini, N.; Belon, P.; Khuda-Bukhsh, A.R. Ascorbic acid combats arsenic-induced oxidative stress in mice liver. *Ecotoxicol Environ Saf*. **2009** Feb;72(2):639-49. doi: 10.1016/j.ecoenv.2008.07.005. Epub 2008 Aug 19. PMID: 18715643
26. Alyoussef, A.; Al-Gayyar, M.M.H. Cytotoxic and partial hepatoprotective activity of sodium ascorbate against hepatocellular carcinoma through inhibition of sulfatase-2 in vivo and in vitro. *Biomed Pharmacother*. **2018** Jul;103:362-372. doi: 10.1016/j.biopha.2018.04.060. Epub 2018 Apr 24. PMID: 29669302
27. Abhilash, P.A.; Harikrishnan, R.; Indira, M. Ascorbic acid supplementation down-regulates the alcohol induced oxidative stress, hepatic stellate cell activation, cytotoxicity and mRNA levels of selected fibrotic genes in guinea pigs. *Free Radic Res*. **2012** Feb;46(2):204-13. doi: 10.3109/10715762.2011.647691. Epub 2012 Jan 23. PMID: 22149461
28. Ishii, N.; Homma, T.; Guo, X.; Yamada, K.I.; Yamada S.; Fujii J. Ascorbic acid prevents N-nitrosodiethylamine-induced hepatic injury and hepatocarcinogenesis in Akr1a-knockout mice. *Toxicol Lett*. **2020** Oct 15;333:192-201. doi: 10.1016/j.toxlet.2020.08.005. Epub 2020 Aug 14. PMID: 32805337
29. Mezni, A.; Khazri, O.; Jarnier, F.; Hardouin, J.; Limam, F.; Jouenne, T.; Aouani, E.; Cosette, P. Hepatoprotective Effect of Grape Seed and Skin Extract Against Lithium Exposure Examined by the Window of Proteomics. *Dose Response*. **2022** Nov 22;20(4):15593258221141585. doi: 10.1177/15593258221141585. eCollection 2022 Oct-Dec. PMID: 36458281
30. Chadha, V.D.; Bhalla, P.; Dhawan, D.K. Zinc modulates lithium-induced hepatotoxicity in rats. *Liver Int*. **2008** Apr;28(4):558-65. doi: 10.1111/j.1478-3231.2008.01674.x. PMID: 18339081
31. Zheng, R.; Liu, K.; Chen, K.; Cao, W.; Cao, L.; Zhang, H.; Sun, H.; Liu, C. Lithium Carbonate in the Treatment of Graves' Disease with ATD-Induced Hepatic Injury or Leukopenia. *Int J Endocrinol*. **2015**;2015:694023. doi: 10.1155/2015/694023. Epub 2015 Oct 20. PMID: 26576153
32. Abdel-Emam, R.A.; Ali, M.F. Effect of l-carnitine supplementation on lead acetate-induced liver cell apoptosis and inflammation: role of caspase-3 and glycogen synthase kinase-3β enzymes. *Life Sci*. **2022** Feb 15;291:120277. doi: 10.1016/j.lfs.2021.120277. PMID: 34979196.
33. Torshin, I.Yu.; Gromova, O.A.; Chuchalin, A.G.; Zhuravlev, Yu.I. Chemoreactome screening of pharmaceutical effects on SARS-CoV-2 and human virome to help decide on drug-based COVID-19

 doi:10.20944/preprints202409.1645.v

therapy. *FARMAKOEKONOMIKA. Modern Pharmacoeconomics and Pharmacoepidemiology*. **2021**; 14 (2): 191-211. (In Russ.) https://doi.org/10.17749/2070-4909/farmakoekonomika.2021.078

34. Torshin, I.Yu, Rudakov, K.V. On the procedures of generation of numerical features over partitions of sets of objects in the problem of predicting numerical target variables. *Pattern Recognition and Image Analysis*. **2019**; 29 (4): 654–67. https://doi.org/10.1134/S1054661819040175
35. Torshin, I.Yu.; Rudakov, K.V. Topological Chemograph Analysis Theory As a Promising Approach to Reproduction Modeling of Quantum-Mechanical Properties of Molecules. Part II: Quantum-Chemical Interpretations of Chemograph Theory. *Pattern Recognition and Image Analysis*, **2021**, Vol. 31, No. 4, pp. 884–896. DOI: 10.1134/S1054661821040258
36. Directive 2010/63/EU of the European Parliament and of the Council of the European Union on the protection of animals used for scientific purposes.